A Neural Adaptive Assisted Backstepping Controller for MPPT in Photovoltaic Applications

Okba Boutebba
Dept.of Electronics
Power electronics and industrial control laboratory (LEPCI),
Sétif, Algeria
boutebbaokba@univ-setif.dz

Antonino Laudani
Dipartimento di Ingegneria
Università degli Studi Roma Tre
Rome, Italy
alaudani@uniroma3.it

Gabriele Maria Lozito
Dipartimento di Ingegneria
Università degli Studi Roma Tre
Rome, Italy
gabrielemaria.lozito@uniroma3.it

Fabio Corti
Dipartimento di Ingegneria
dell'Informazione (DINFO)
Università degli Studi di Firenze
Firenze, Italy
fabio.corti@unifi.it

Alberto Reatti
Dipartimento di Ingegneria
dell'Informazione (DINFO)
Università degli Studi di Firenze
Firenze, Italy
alberto.reatti@unifi.it

Samia Semcheddine
Dept.of Electronics
Power electronics and industrial control laboratory (LEPCI),
Sétif, Algeria
samia.semchedine@univ-setif.dz

***Abstract*—Maximum power point tracking is a key asset to ensure an efficient energy conversion when a photovoltaic power source is involved. In this work, a novel approach combining a Neural-Network based tracking technique with an highly efficient algorithm for non-inverting buck-boost DC-DC converter (NIBB) control is proposed. The approach is validated through comparison against the well-known P&O algorithm, resulting superior both in terms of identifying the correct operating point for the PV device, and in terms of dynamic stability of the converter.**

Keywords—Maximum Power Point Tracking, Photovoltaics, DC-DC Converters, Neural Networks, Adaptive backstepping, Single-Diode Model

I. INTRODUCTION

Reliance on photovoltaic (PV) devices as power-supply is found at all different scales, from small applications such as stand-alone electronics equipment, to power-grid injection by means of inverters. Still, the non-linear nature of the PV device, and the strong influence that environmental quantities such as irradiance (G) and temperature (T) have on its electrical characteristics, require DC-DC conversion stages with advanced control algorithms for Maximum Power Point Tracking (MPPT). The goal of an MPPT algorithm is to determine the optimal operating point for the PV device where the delivered power form the device to the load is maximum.

The MPPT converter is, in general, directly interfaced with the DC-DC converter, since the equivalent load seen from the PV device (responsible for the load-line and the operating point) is a function of the DC-DC duty cycle. A very common MPPT algorithm that is found in several commercial DC-DC converters for PV application is the P&O. This algorithm perturbs the operating point of the PV device and measures the variation in the delivered power. From this perturbation, the optimal direction of variation (increasing or decreasing the duty-cycle) is determined. The P&O is very popular for its simplicity of implementation without any a-priori knowledge of the PV device itself. However, it lacks in convergence speed and stability when large transients are involved. The approach proposed in this work make use of a suitably trained Artificial Neural Network (ANN) to determine the optimal operating point of the PV device. The ANN is trained using a dataset obtained by the well-known Single-Diode Model for silicon PV devices. Once the optimal operating point is found, the optimal value for the converter duty cycle must be reached. This operation is performed by means of a very efficient controller adaptive backstepping (*ABSC*), the basic idea of this later is used to design stable controls with a recursive methodology. It must stabilize the origin of a system by means of closed loop control laws and using Lyapunov functions to ensure the stability of the system [1-4].

The neural MPPT estimator along with the adaptive backstepping controller (*ABSC*) create a Neural DC-DC controller that can quickly and accurately tune the duty-cycle to ensure optimal delivered power even in presence of rapidly and slowly changing environmental conditions.

The approach is validated in Simulink environment on a simple Non-Inverting Buck-Boost (NIBB) converter topology[5-6] with a PV power source and a resistive load. The environmental conditions of irradiance and temperature on the PV device are considered in different scenarios, either constant, slowly changing or abruptly changing. The accuracy of the controller is compared against a classic controller found in commercial devices composed by a P&O MPPT and a simple PI (Proportional-Integral) controller, *P&O/ABSC* and *ANN/PI*.

The paper will be structured as follows. In the second section, the neural MPPT approach will be described in detail, with insight on the ANN architecture, dataset creation and training. In the third section, the ABSC algorithm will be discussed, with special focus on the practical implementation for PV devices. In the fourth section, the Simulink comparison versus the classic *P&O/PI* controller, *ANN/PI* and *P&O/ABSC* will be presented. Conclusions and final remarks will close the paper.

II. A NEURAL APPROACH FOR MPPT

Solving a control problem with the aid of an ANN is, in general, a task involving three steps. The first one is, given the system to be controlled, to identify the desired quantity to be

978-1-7281-7455-6/20/$31.00 ©2020 IEEE

estimated by the ANN, and all the input variables required to estimate it, thus defining the functional relationship between input and output. The second one is to create, through the use of an equivalent model, a very large dataset where the quantities are arranged in terms of input samples and output samples. The third step is the creation and training of the ANN on the previously created dataset, eventually saving some samples for an independent validation check. For the first step, the quantity to be estimated is the optimal operating point for the PV device. Although this operating point is defined by a current (i_{mp}) and a voltage (v_{mp}), only one is a necessary quantity for a DC-DC controller. In this approach, only the optimal voltage is going to be estimated by the ANN. Several approaches use different candidate inputs (mostly related to climatic conditions) to estimate the v_{mp}, however, a successful methodology, previously used [7], involves the measurement of the actual (i.e. non-optimal) operating point of the PV device (v_{pv}, i_{pv}) , and its temperature (T). Thus, the functional relationship to be learnt by the ANN is the following

$$V_{mp} = f\ (V_{PV}\ , I_{PV}\ , T\ ) \tag{1}$$

For the second step, a dataset of triplets (v_{pv}, i_{pv}, T) and the relative v_{mp} must be created. The dataset must be representative of the system, and for this reason, it must be acquired in all the possible (and sensible) conditions for the PV device. A set of N_G = 15 irradiance values between 100W/m2 and N_T = 15 temperatures between 263.15K and 365K. Each individual combination N_G-N_T is used to create an I-V curve of the PV device by means of the One-Diode model, extracting the v_{mp} optimal voltage. The parameters of the One-Diode model were obtained through model identification from *BP MSX 120* and are reported in Tab. I, where R_S is the series resistance, R_{SH} is the shunt resistance, I_{irr} is the photocurrent, I_o is the diode reverse saturation current, and n is the diode ideality factor.

TABLE I. DIODE MODEL PARAMETERS

Parameter	Symbol	Values
Series Resistance	R_S	0.433 Ω
Shunt Resistance	R_{SH}	415.4 Ω
Reverse Saturation Current	I_o	3.870 A
Photocurrent	I_{irr}	9.65×10^{-8} A
Ideality Factor	n	1.3

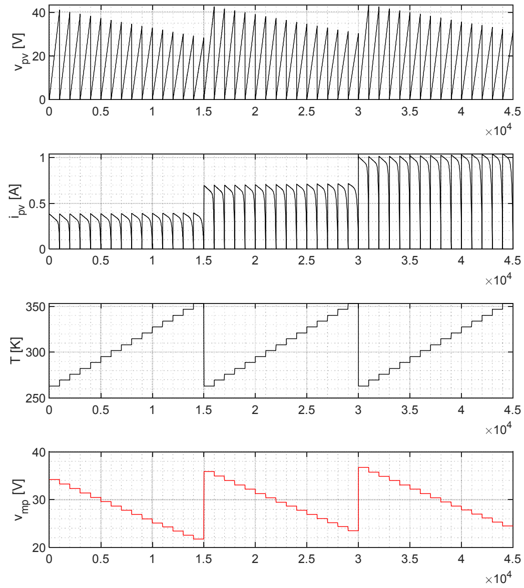

Fig. 1. Portion of the dataset for the training of the ANN. First three plots in black show the input data (v_{pv}, i_{pv}, T). Last plot in red shows the output data v_{mp}.

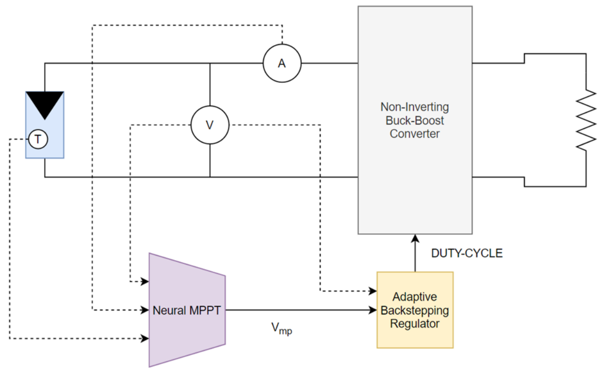

Fig. 2. Connection scheme for the Neural MPPT estimator. Circles represent sensors for temperature, current and voltage of the PV panel.

Considering N_S = 1000 points per I-V curve, the dataset size used for the training is composed of $N_G \times N_T \times N_S$=225000 input-output samples. The portion of the dataset is shown in Fig. 1. An additional, smaller dataset, of 10000 samples, was created for independent validation.

For the third step, this problem was already solved successfully in previous works using a single-layer feed-forward architecture. The network was sized according to an empiric procedure based on a comparison between the training error on different datasets and the number of neurons in the hidden layer. The optimal number of neurons found for the network is 10, with a mean-square-error at the end of the training procedure lower than 10^{-3}.

The ANN MPPT estimator connection scheme with is shown in Fig. 2.

III. Non-Inverting Buck-Boost Adaptive Backstepping Controller

To obtain the optimal reference voltage, the ANN is used to extract the condition of maximum delivered energy from the photovoltaic generator. On the other hand, a non-linear adaptive backstepping aims to track this reference voltage of the photovoltaic generator by controlling the duty cycle μ of the NIBB power converter.

This proposed control is based on the fact that the inductance L and capacitor C_1 of the NIBB converter are either unknown or have variations. Therefore, this control may be used for NIBB converters regardless of the parameter values, due to its learning capability to solve the model uncertainty through online estimation of the unknown or changeable parameters. The dynamic model of the NIBB converter in term of duty cycle ‘‘μ’’ is given by using the averaging method presented in [5-6], and that appears in equation (2)

$$\begin{cases} \dot{x}_1 = \dot{V}_{PV} = \frac{1}{\theta}.I_{PV} - \frac{1}{\theta}\mu.x_2 \\ \dot{x}_2 = \dot{I}_L = -\Phi x_3 + \Phi\mu.(x_1 + x_3) \\ \dot{x}_3 = \dot{V}_S = \frac{x_2}{C_2} - \frac{x_3}{RC_2} - \mu\frac{x_2}{C_2} \end{cases} \tag{2}$$

Where $\theta = C$, $\Phi = 1/L$, and it is also important to take in consideration that the parameter $\psi = 1/C_1$ used to facilitate the calculations. So, the calculation of the control law must be done in several steps while ensuring stability.

Step 1: Find, a virtual control law

To be able start the controller design it is necessary to define the error signal, which is defined as the difference between the actual voltage V_{PV} and the voltage reference

$$e_1 = x_1 - x_{1\_ref} \tag{3}$$

where x_{1_ref} is the voltage reference produced by the ANN algorithm. Assuming convergence of the voltage error ($e_1 = 0$), we can achieve in a simple manner the desired result. Using equations (3), the tracking error derivative is written as follows

$$\dot{e}_1 = \frac{1}{\theta}.I_{PV} - \frac{1}{\theta}\mu.x_2 - \dot{x}_{1\_ref} \tag{4}$$

The following Lyapunov function is considered by

$$V_1 = \frac{1}{2}e_1^2 \tag{5}$$

To verify and assure the asymptotic stability, the Lyapunov function must be positive $V_1>0$ and its derivative with respect to time must be negative $V_1<0$ definite. Taking the time derivative of equation (5), we get

$$\dot{V}_1 = e_1\dot{e}_1 \tag{6}$$

$$\dot{V}_1 = e_1\left(\frac{1}{\theta}.I_{PV} - \frac{1}{\theta}\mu.x_2 - \dot{x}_{1\_ref}\right) \tag{7}$$

From the derivative of Lyapunov function, V_1 is negative if

$$\frac{1}{\theta}.I_{PV} - \frac{1}{\theta}\mu.x_2 - \dot{x}_{1\_ref} = -K_1.e_1 \tag{8}$$

At this point, we can defined and write the virtual control law (the function of stabilization) as follows

$$x_2 = \beta = \frac{1}{\mu}\left(I_{PV} - \theta.\dot{x}_{1\_ref} + \theta.K_1.e_1\right) \tag{9}$$

Using the values of $\boldsymbol{x_2}$ from (9)**,** Eq. (6) becomes

$$\dot{V}_1 = -K_1 e_1^2 \tag{10}$$

The derivative of V_1 is definitively negative if K_1 is positive, moreover, equation (6) must be satisfied. Therefore, the asymptotic stability of the system given by equation (2) in origin is reached.

Step 2: Find μ, the original control input

The second error variable, which represent the difference between the state variable $x_2 = I_L$ and its desired value $x_{2\_ref}=\beta$, is defined by

$$e_2 = x_2 - \beta \tag{11}$$

By Differentiating (11), Equation (4) becomes

$$\dot{e}_1 = -K_1.e_1 - \frac{e_2}{\theta}\mu \tag{12}$$

The derivative of $\boldsymbol{e_2}$ can be defined as follows

$$\dot{e}_2 = \dot{x}_2 - \dot{\beta} \tag{13}$$

Therefore,

$$\begin{aligned} \dot{e}_2 = {} & -\Phi x_3 + \Phi\mu.(x_1 + x_3) + K_1.e_2 + \frac{\theta.K_1^2 e_1}{\mu} - \frac{\dot{\theta}.K_1 e_1}{\mu} \\ & - \frac{\dot{I}_{PV}}{\mu} + \frac{\dot{\theta}\dot{x}_{1\_ref}}{\mu} + \frac{\theta.\ddot{x}_{1\_ref}}{\mu} + \frac{\dot{\mu}}{\mu}\beta \end{aligned} \tag{14}$$

To ensure the asymptotic stability and the convergence of the errors $(e_1, e_2) = (0,0)$, a composite Lyapunov function V_t is defined whose time derivative must be negative and definite for all the values of x_1 and x_2 [8-9].

$$Vt = V_1 + \frac{1}{2}e_2^2 \tag{15}$$

The derivative of V_t is

$$\dot{V}t = -K_1 e_1^2 + e_2\left(\dot{e}_2 - \frac{e_1}{\theta}\mu\right) \tag{16}$$

$$\dot{V}t = -K_1 e_1^2 + e_2\left(-\Phi x_3 + \Phi\mu.(x_1 + x_3) + K_1 e_2 - \frac{\dot{I}_{PV}}{\mu}\right)$$
$$+ e_2\left(\frac{\theta.K_1^2 e_1}{\mu} - \frac{\dot{\theta}.K_1 e_1}{\mu} + \frac{\dot{\theta}\dot{x}_{1\_ref}}{\mu} + \frac{\theta\ddot{x}_{1\_ref}}{\mu} - \frac{e_1}{\theta}\mu + \frac{\dot{\mu}}{\mu}\hat{\beta}\right) \quad (17)$$

To ensure that the value $\dot{V}_t$ negative, it is necessary to verify

$$\dot{e}_2 - \frac{e_1}{\theta}.\mu = -K_2 e_2 \quad (18)$$

from equation (18) we can get

$$\dot{\mu} = \frac{1}{\hat{\beta}}\left(\dot{\hat{\theta}}.K_1 e_1 - \hat{\theta}.K_1^2 e_1 - \mu K_2 e_2 - \mu.K_1 e_2 + \dot{I}_{PV}\right)$$
$$+ \frac{1}{\hat{\beta}}\left(\hat{\Phi}.\mu.x_3 - \hat{\Phi}\mu^2.(x_1 + x_3) - \dot{\hat{\theta}}\dot{x}_{1\_ref} - \hat{\theta}\ddot{x}_{1\_ref} + \frac{e_1}{\hat{\theta}}\mu^2\right) \quad (19)$$

where μ=[0,1] , $\hat{\psi}$, $\hat{\theta}$ and $\hat{\Phi}$ are the estimated parameters. The errors are described (20).

$$\begin{cases} \Psi = \hat{\Psi} + \tilde{\Psi} \\ \theta = \hat{\theta} + \tilde{\theta} \\ \Phi = \hat{\Phi} + \tilde{\Phi} \end{cases} \quad (20)$$

Now, replacing (20) in (17), yields (21) after some algebraic manipulations and replacing the estimation parameters by the errors.

$$\dot{V}t = -K_1 e_1^2 - K_2 e_2^2 - \tilde{\Phi} x_3 e_2 + \mu.(x_1 + x_3)\tilde{\Phi} e_2 - e_1 e_2.\mu.\tilde{\Psi}$$
$$+ \frac{K_1^2 e_1}{\mu}\tilde{\theta} e_2 - \frac{K_1 e_1}{\mu}\dot{\tilde{\theta}} e_2 + \frac{\dot{x}_{1\_ref}}{\mu}\dot{\tilde{\theta}} e_2 + \frac{\ddot{x}_{1\_ref}}{\mu}\tilde{\theta} e_2 \quad (21)$$

Different Lyapunov functions must be defined so as to achieve parameter adaptation laws for $\hat{\Phi}$, $\hat{\theta}$ and $\hat{\Psi}$

$$\begin{cases} V_3 = \frac{1}{2\xi}\tilde{\Phi}^2 \\ V_4 = \frac{1}{2\Delta}\tilde{\theta}^2 \\ V_5 = \frac{1}{2.T}\tilde{\Psi}^2 \end{cases} \quad (22)$$

where ζ, Δ and T, are constants and positive.

Finally, the global Lyapunov function is shown in (23).

$$Vg = V_t + V_3 + V_4 + V_5 \quad (23)$$

The derivative of Vg is

$$\dot{V}g = -K_1 e_1^2 - K_2 e_2^2$$
$$+ \left(-x_3 e_2 + \mu.(x_1 + x_3)e_2 - \frac{1}{\xi}\dot{\hat{\Phi}}\right)\tilde{\Phi}$$
$$+ \left(-e_1 e_2.\mu - \frac{1}{T}\dot{\hat{\Psi}}\right)\tilde{\Psi} \quad (24)$$
$$+ \left(+\frac{K_1^2 e_1}{\mu}e_2 + \frac{\ddot{x}_{1\_ref}}{\mu}e_2 - \frac{1}{\Delta}\dot{\hat{\theta}}\right)\tilde{\theta}$$

Thus, in order to make the state vector vanish asymptotically, the terms with the estimation parameters must be cancelled.

$$\dot{\hat{\Phi}} = \xi\left[-x_3 + \mu.(x_1 + x_3)\right]e_2$$
$$\dot{\hat{\Psi}} = T\left[-e_1 e_2.\mu\right] \quad (25)$$
$$\dot{\hat{\theta}} = \Delta\left[K_1^2 e_1 + \ddot{x}_{1\_ref}\right]\frac{e_2}{\mu}$$

IV. SIMULATION RESULTS

Numerical simulation of the photovoltaic chain shown in Fig. 2 is developed and implemented in MATLAB Simulink® environment. The photovoltaic array considered in this work consists of one PV panel. The parameters of this later, the NIBB chopper and the *ABSC* are indicated in Table II. Concerning the NIBB converter, all the components are assumed ideal at first instance. The parasitic resistance of the passive components is taken into account in the simulation as it can influence the system performance [10-11].

	Parameters	***Values***
PV panel	Maximum power (P_{Mpp})	120 W
	Open circuit voltage (V_{OC})	42.1 V
	Short circuit current (I_{SC})	3.87 A
	Voltage at P_{Max} (V_{Mpp})	33.7 V
	Current at P_{Max} (I_{Mpp})	3.56 A
	Number of cells connected in series (N_S)	72
	Number of cells connected in parallel (N_P)	1
NIBB converter	Input capacitor C_1	2200 µF
	Parasitic resistance of Input Capacitor r_{C1}	0.05 Ω
	Output capacitor C_2	1100 µF
	Parasitic resistance of Input Capacitor r_{C2}	0.05 Ω
	Inductor L	10 mH
	Inductor Parasitic resistance r_L	0.05 Ω
	Load R	50 Ω
ABSC controller	K_1	7e3
	K_2	100

The studied system is tested firstly, under gradual and sudden change in solar irradiation as shown in Fig. 3 and a fixed temperature of T=25 ◦C.

As shown by the simulations, during the variation of each irradiance level, the proposed *ANN/ABSC* tracks successfully the reference voltage $V_{PV\text{-}ref}$ as shown in Fig.4. The performance of the proposed controller is then confirmed.

Fig. 5. Illustrates the results obtained for the overall power of the photovoltaic generator with the proposed control *ANN/ABSC* and compared with the classical *ANN/PI* controller. It can be observed that the proposed controller has a very high performance at any level of irradiation changes and the controller performed well.

Fig.5. shows the convergence of the error signal e_1 to zero below the sudden and gradual irradiance variations.

In this second test, the irradiation level is permanently fixed at G = 1 kW/m² and the temperature is change as shown in Fig.7 . The profile starts at a value of 25°C; during the first time interval [0.5 – 1] sec, the temperature gradually increases from 25°C to 65°C. Then, four consecutive step changes are made: (65–35), (35–45), (45–35) and (35–65) °C. Finally, the level of temperature gradually decreases from 65 to 25 °C.

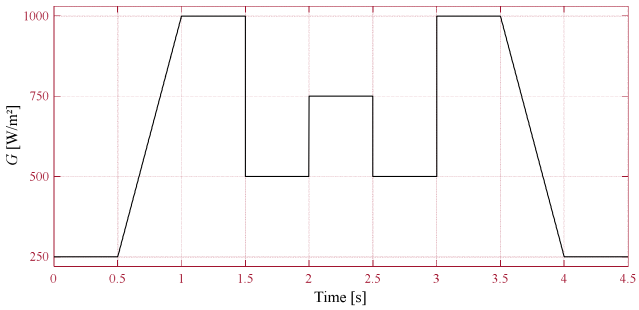

Fig. 3. Solar Irradiance profile.

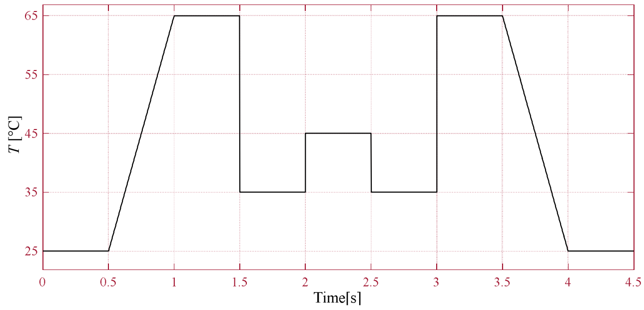

Fig. 7. Temperature profile.

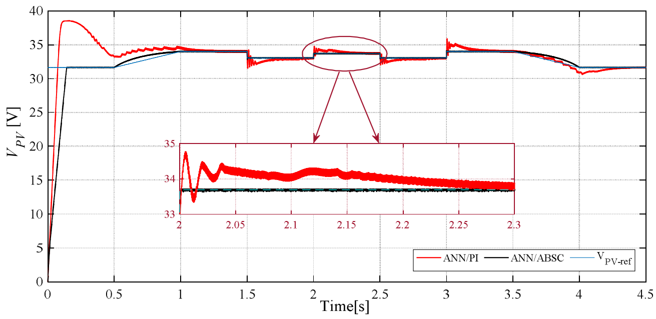

Fig. 4. Simulated PV voltage with ANN/ABSC and ANN/PI methods.

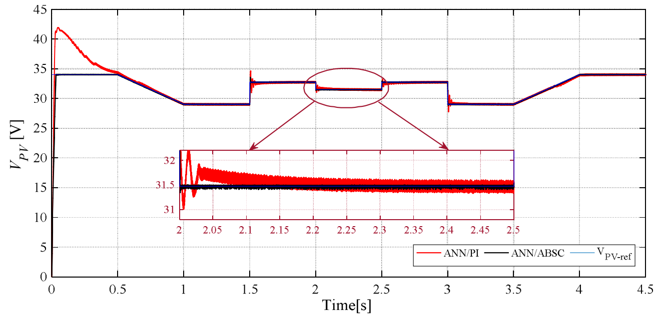

Fig. 8. Tracking of V_{PV} for different levels of temperature

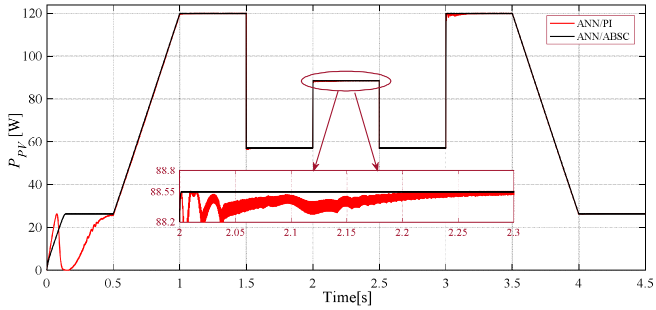

Fig. 5. Simulated PV power with ANN/ABSC (black) and ANN/PI (red) methods for different values of solar irradiation.

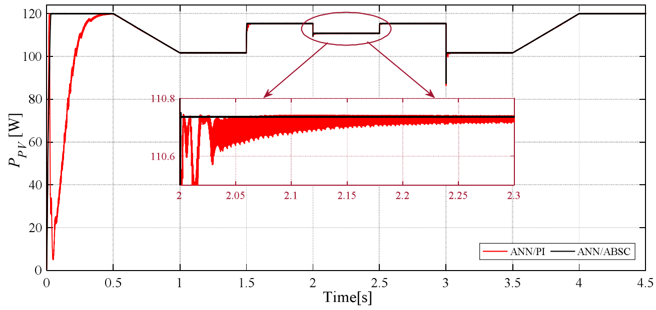

Fig. 9. Power of PV array with ANN/ABSC ((black) and ANN/PI (red) methods for different levels of temperature

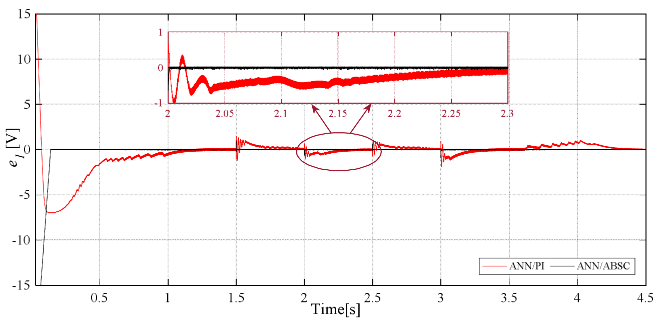

Fig. 6. Error signal e_1 under varying irradiance .

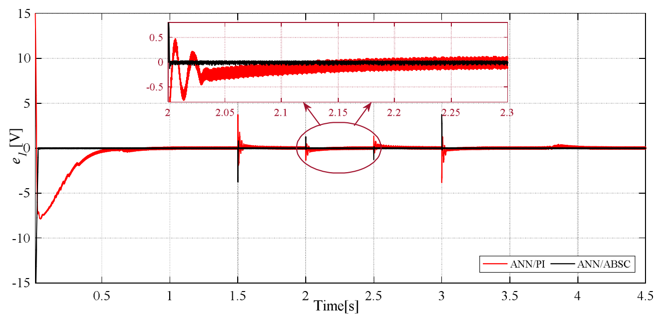

Fig. 10. Error signal e1 under varying temperature .

From photovoltaic array curves, the performance of the proposed control *ANN/ABSC* is again confirmed with good tracking to $V_{PV\text{-}ref}$, as shown in Fig. 8. Thus, power P_{PV} achieves the MPPT at the same time as shown at Fig.9. Moreover, one can deduce that the proposed *ANN/ABSC* presents a good transition response, and a very fast system reaction against set point change.

Fig. 10 shows the convergence of the error signal e_1 to a null value under the variation of temperature, with a low fluctuation.

To show the performance of the proposed MPPT (*ANN/ABSC)*, results obtained in this paper are compared with those achievable by the classical *P&O/PI* controller and *P&O/ABSC*. The comparison is based on simulations using the same temperature and irradiation changes than those used in previous results for the *ANN/ABCS* and *ANN/PI*. Also sampling time and PWM frequency are the same levels. Fig.11 and 12 shows the dynamic response of PV power for the conventional P&O/PI, P&O/ABSC and proposed MPPT ANN/ABSC techniques controller respectively. Firstly, we consider the irradiation level and temperature levels is suddenly .

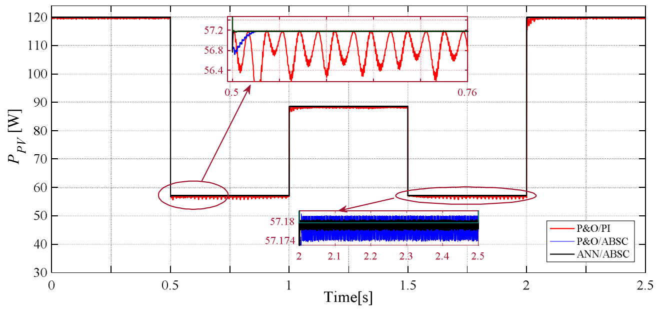

Fig. 11. PV power: conventional P&O/PI (red), P&O/ABSC (bleu) and proposed ANN/ABSC (black) under sudenly irrdiation change.

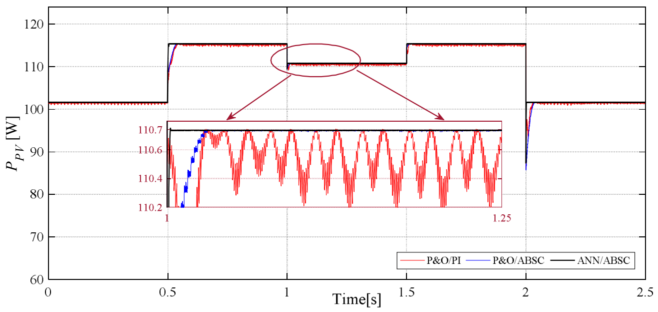

Fig. 12. PV power waveforms for: conventional P&O (black), P&O/PI (red) and proposed P&O/AIDSM (blue) under sudenly temperature change.

The P_{PV} power with conventional methods fluctuates around the reference $P_{PV\text{-}ref}$, while for the proposed *ANN/ABSC*, the P_{PV} v tracks accurately its reference in a much narrower voltage range. Moreover, the *ANN/ABSC* reaches the MPP more rapidly than the P&O/PI and *P&O/ABSC*, and also, during the variation of environmental condition levels, the proposed controller (*ANN/ABSC*) results provides more valuable in terms of a lower maximum overshoots, response time and oscillations are very low if compared with the classical methods.

V. Conclusions

An efficient approach for a fast and reliable MPPT controller in PV applications was proposed. The approach is based on the combination of a neural-based estimator for the optimal operating point of the PV device with an adaptive algorithm for duty-cycle control. The approach was compared against a standard approach composed by a simple PI controller driven by a Perturb & Observe search algorithm, which is found in different variations for several field-related applications [12-14]. Both approaches were implemented in Simulink environment along with a NIBB converter to validate their capabilities in a real dynamic simulation, considering rapidly varying conditions of irradiance and temperature. The comparison shows that the proposed approach features quicker convergence, smaller oscillations around the optimal point, and is less prone to instabilities and overshoot in case of large transients. The practical implementation of the control approach proposed, coupled with the computational simplicity of the ANN used, makes this approach suitable for high-performance implementation on microcontrollers and FPGA units [15-18].

References

[1] O. S. Bhatti, U. T. Shami, K. Mahmood-ul-Hasan, F. Abbas, et S. Mahmood, " Robust-Optimal Output-Voltage Control of Buck Converter using Fuzzy Adaptive Weighted Combination of Linear Feedback Controllers", *J. Control Eng. Appl. Inform.*, vol. 21, nº 2, p. 43–53, 2019.

[2] O. Boutebba, S. Semcheddine, F. Krim, et B. Talbi, "Adaptive Nonlinear Controller Design for DC-DC Buck Converter via Backstepping Methodology", in 2019 International Conference on Advanced Electrical Engineering (ICAEE), 2019, p. 1–7.

[3] O. Boutebba, S. Semcheddine, F. Krim, et B. Talbi, "Design of a Backstepping-Controlled Boost Converter for MPPT in PV Chains", in *2019 International Conference on Advanced Electrical Engineering (ICAEE)*, 2019, p. 1–7.

[4] H. Al-Baidhani, M. K. Kazimierczuk, T. Salvatierra, A. Reatti and F. Corti, "Sliding-Mode Voltage Control of Dynamic Power Supply for CCM," *2019 IEEE International Symposium on Circuits and Systems (ISCAS)*, Sapporo, Japan, 2019, pp. 1-5.

[5] X. Weng *et al.*, "Comprehensive comparison and analysis of non-inverting buck boost and conventional buck boost converters", *J. Eng.*, vol. 2019, nº 16, p. 3030–3034, 2019.

[6] Y. S. Joel, H. V. Saikumar, et S. S. R. Patange, "Design & performance analysis of Fuzzy based MPPT control using two-switch non inverting Buck-Boost converter", in *2016 International Conference on Electrical Power and Energy Systems (ICEPES)*, 2016, p. 414–419.

[7] Lozito, G. M., Bozzoli, L., & Salvini, A. (2014, September). Microcontroller based maximum power point tracking through FCC and MLP neural networks. In 2014 6th European Embedded Design in Education and Research Conference (EDERC) (pp. 207-211). IEEE.

[8] H. K. Khalil et J. W. Grizzle, *Nonlinear systems*, vol. 3. Prentice hall Upper Saddle River, NJ, 2002.

[9] N. H. McClamroch, "Stability of Dynamical Systems-On the Role of Monotonic and Non-Monotonic Lyapunov Functions", *IEEE Control Syst. Mag.*, vol. 36, nº 1, p. 77–78, 2016.

[10] A. Reatti, F. Corti, A. Tesi, A. Torlai and M. K. Kazimierczuk, "Effect of Parasitic Components on Dynamic Performance of Power Stages of DC-DC PWM Buck and Boost Converters in CCM," *2019 IEEE International Symposium on Circuits and Systems (ISCAS)*, Sapporo, Japan, 2019, pp. 1-5.

[11] E. Locorotondo, L. Pugi, F. Corti, L. Becchi and F. Grasso, "Analytical Model of Power MOSFET Switching Losses due to Parasitic Components," *2019 IEEE 5th International forum on Research and Technology for Society and Industry (RTSI)*, Florence, Italy, 2019, pp. 331-336.

[12] Cheddadi, Y., Errahimi, F., & Es-sbai,. "Design and verification of photovoltaic MPPT algorithm as an automotive-based embedded software",Solar Energy, N. (2018) 171, 414-425.

[13] Sarigiannidis, A. G., Stathis, S. A., & Kladas, A. G., "Performance evaluation of MPPT techniques for PV array incorporated into electric vehicle roof", International Conference on Renewable Energy Research and Applications (ICRERA), pp. 1069-1073, November 2015.

[14] Killi, M., & Samanta, S., "Modified perturb and observe MPPT algorithm for drift avoidance in photovoltaic systems", IEEE transactions on Industrial Electronics, 62(9), pp.5549-5559.

[15] Laudani, A., Lozito, G. M., Fulginei, F. R., & Salvini, " An efficient architecture for floating point based MISO neural neworks on FPGA", 16th International Conference on Computer Modelling and Simulation pp. 12-17.

[16] Mellit, A., Rezzouk, H., Messai, A., & Medjahed, "FPGA-based real time implementation of MPPT-controller for photovoltaic systems", Renewable energy, 36(5), pp.1652-1661.

[17] Laudani, A., Fulginei, F. R., Salvini, A., Lozito, G. M., & Mancilla-David, F., "Implementation of a neural MPPT algorithm on a low-cost 8-bit microcontroller" , International Symposium on Power Electronics, Electrical Drives, Automation and Motion, pp. 977-981, June 2014.

[18] Khaehintung, N., Wiangtong, T., & Sirisuk, P., "FPGA implementation of MPPT using variable step-size P&O algorithm for PV applications", International Symposium on Communications and Information Technologies, pp. 212-215, October 2006.